DIRAC-NOTE-2011-03

THE NEW PRESHOWER DETECTOR FOR DIRAC-II SET-UP

Characteristics and Performances

M.Pentia, S.Constantinescu, M.Gugiu

1. Characteristics of the new preshower detector

PSh detector samples the early, good shape part (1- $6X_0$) of the electron shower (see **Figure 1**), before the pion shower is initiated. Therefore the PSh detector has a high amplitude spectrum for electrons and low amplitude for pions. This provides the electron/pion separation.

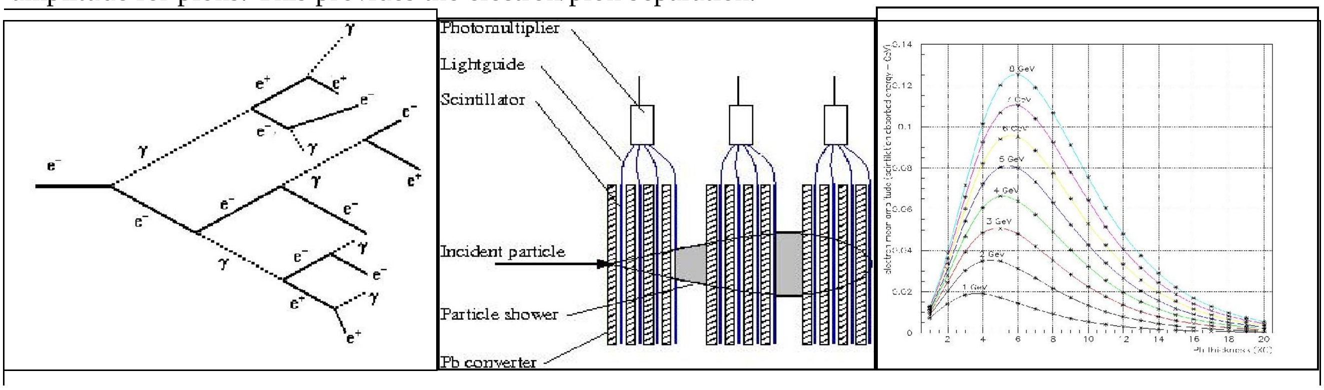

Figure 1. Development of the electromagnetic shower and longitudinal distribution of the transfer energy.

The geometrical characteristics of the new preshower detector are presented in **Figure 2.** It contains, as first layer, a Pb converter of 10*mm* thickness for the first two slabs and 25*mm* for the rest. The second layer, placed behind the first one, in the kaon flight region. It contains Pb converter slabs of 10*mm* thickness. The detector slabs, placed behind the Pb converter, are plastic scintillators BICRON type 408 of 10*mm* thickness.

The two arms PSh detector layout along with the DIRAC setup is presented in **Figure 3.**

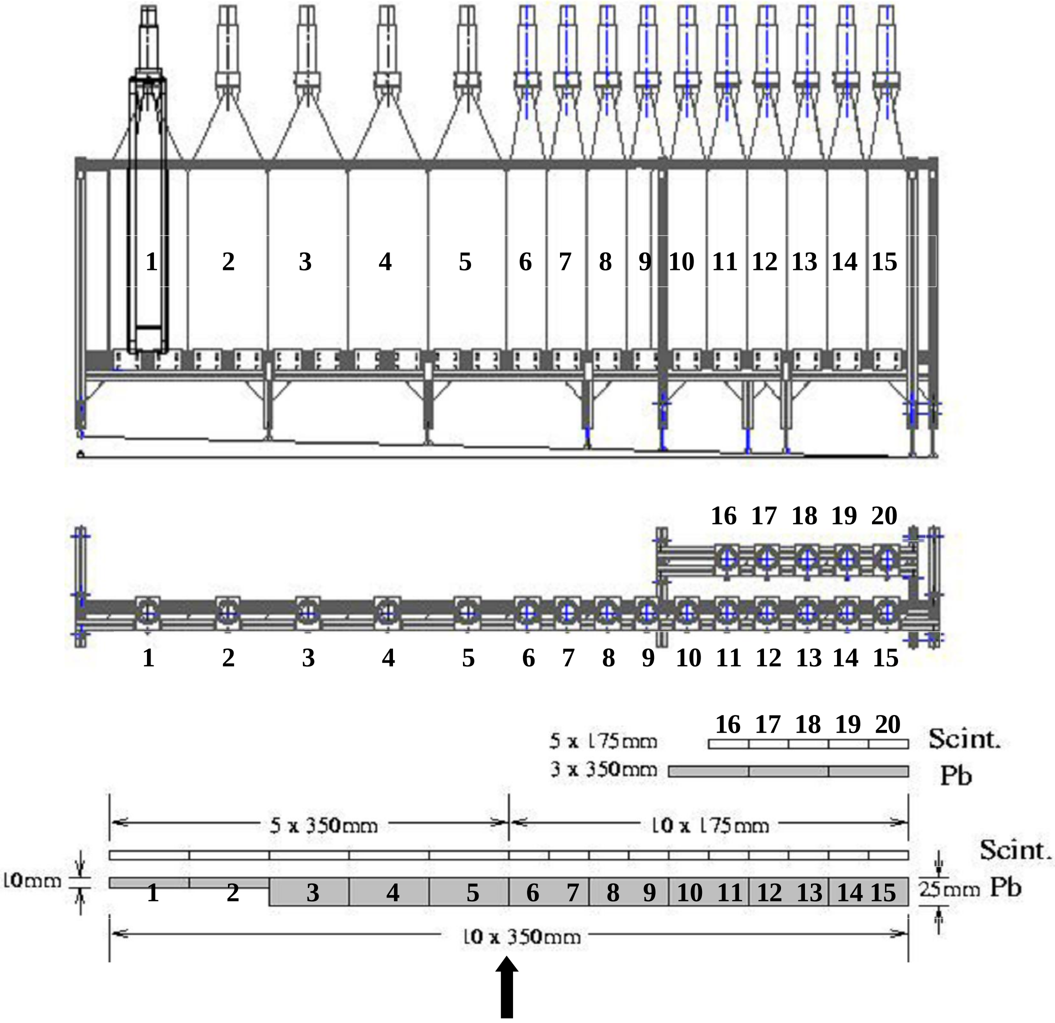

Figure 2. The preshower left arm geometry and structure.

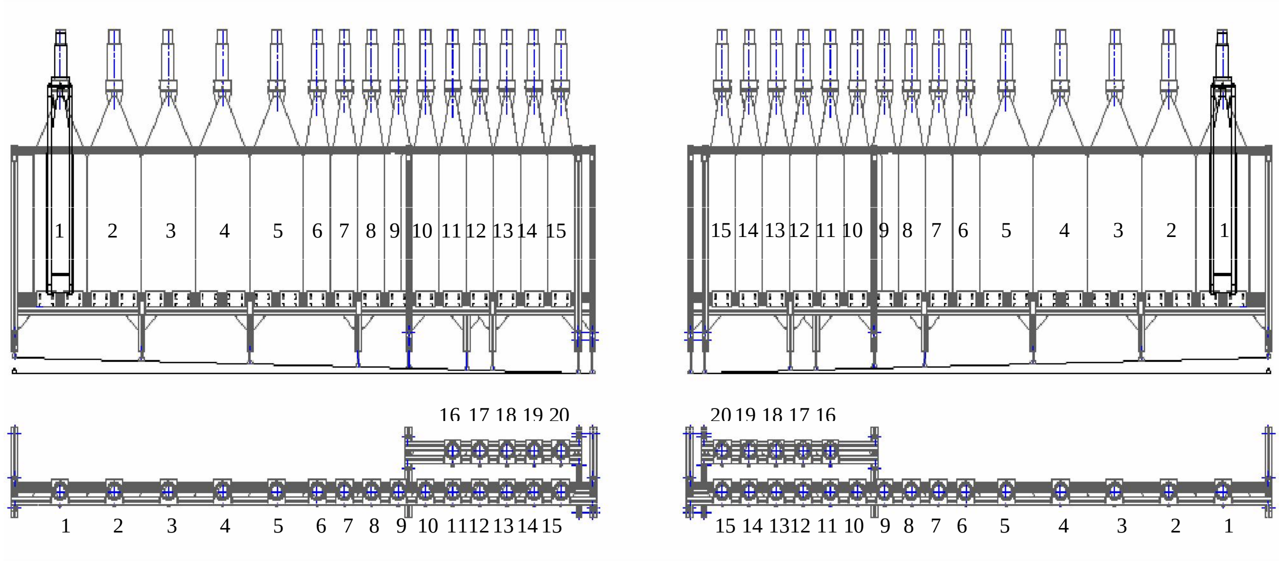

Figure 3. The layout of the two arm PSh arrangement within DIRAC setup.

Figure 4. Preshower left arm in the DIRAC set-up

The PSh detector has been extended to include the phase space of the kaon flight detection region. Here, to compensate for the smaller electron rejection efficiency of the Nitrogen Cherenkov, the PSh detector has been built up with two layers.

2. One layer preshower detector efficiency

The typical PSh amplitude spectra, for pions and electrons, are presented in **Figures 5** and **6.** They are registered in anticoincidence and coincidence with the Nitrogen Cherenkov detector signals.

The *e-π* cut channel separation is placed between the pion and electron amplitude distribution spectra. It is used to define the following quantities:

- **pion detection efficiency** (π_{eff}) – the ratio of the cut left side (A_1^{π}) events and the total *pion spectra* events (A_{tot}^{π}):

$$\pi_{eff} = \frac{A_1^{\pi}}{A_{tot}^{\pi}}$$

- **pion loss** (π_{loss}) – the ratio of the cut right side (A_2^{π}) events and the total *pion spectra* events (A_{tot}^{π}):

$$\pi_{loss} = \frac{A_2^{\pi}}{A_{tot}^{\pi}}$$

- **electron rejection** (ε_{rej}) – the ratio of the cut right side (A_2^{el}) events and the total *electron spectra* events (A_{tot}^{el}):

$$\varepsilon_{rej} = \frac{A_2^{el}}{A_{tot}^{el}}$$

- **electron escape** (ε_{esc}) – the ratio of the cut left side (A_1^{el}) events and the total *electron spectra* events (A_{tot}^{el}):

$$\varepsilon_{esc} = \frac{A_1^{el}}{A_{tot}^{el}}$$

2.1. Pion detection and electron rejection efficiency evaluation.

The experimental PSh spectra measurements along the DIRAC setup, using pion and electron trigger, have been registered for every PSh detector slab. The pion peak is practically independent on energy (it is a minimum ionising particle). Therefore we used this peak in the amplitude spectra calibration, by placing the pion peak at the quasi-same position in each spectrum. Nevertheless, it is difficult to have in this way a very good amplitude calibration because the pion peak is just at the begining of the spectra.

Figure 5 showes pion and electron spectra for the slab number 4, 9 and 13 of the right arm (negative particles) and in **Figure 6** are the same slab number spectra of the left arm (positive particles).

The cut channel position has been determined by a Gaussian fit of the pion peak, placed at the 7σ distance on the right side. This was taken by eye evaluation.

Note ! As the energy increases (the slab number increase), pion signals are present also in the PSh electron spectra (see **Figures 5** and **6**). It means that at higher energies the pions produce also Cherenkov radiation, and the Cherenkov detector cannot separate efficiently the electron and pion signals, therefore the electron rejection efficiency is poor. Additional electron-pion separation capability of the PSh detector is essential for a better electron rejection efficiency.

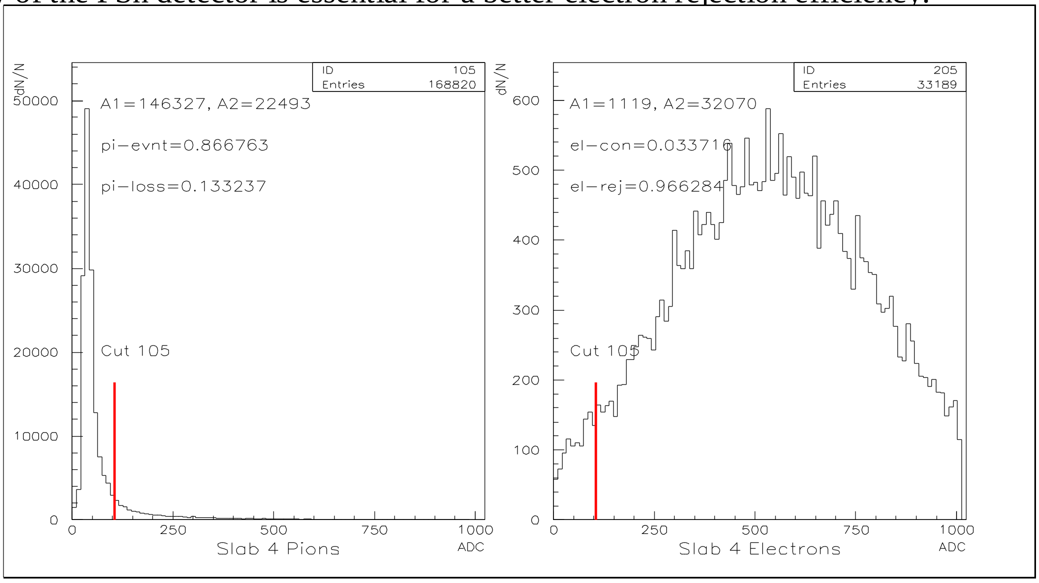

Figura 5 a. PSh Pion and Electron spectra, slab 4, right arm

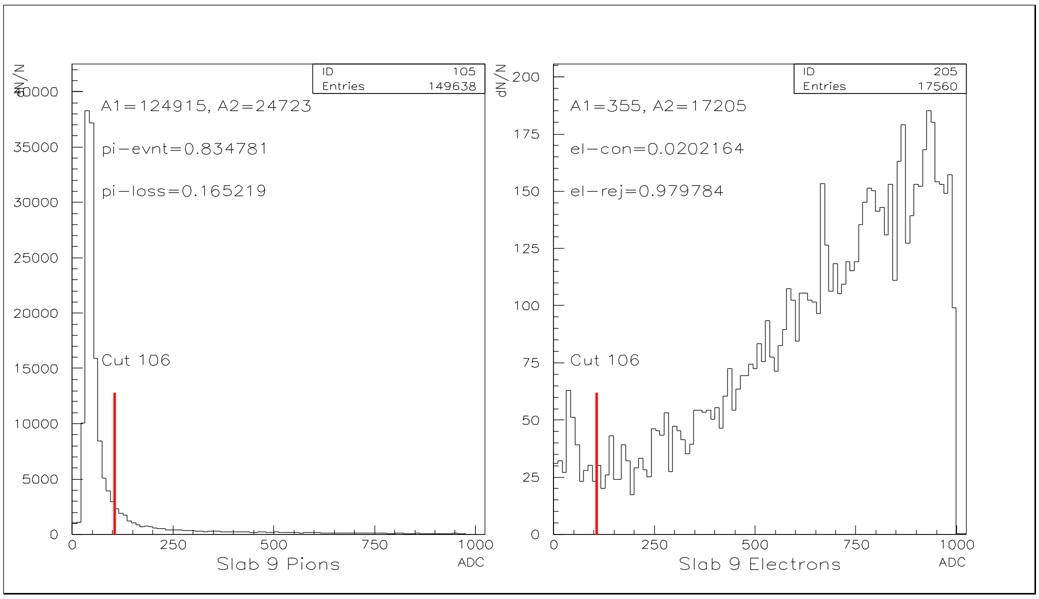

Figura 5 b. PSh Pion and Electron spectra, slab 9, right arm

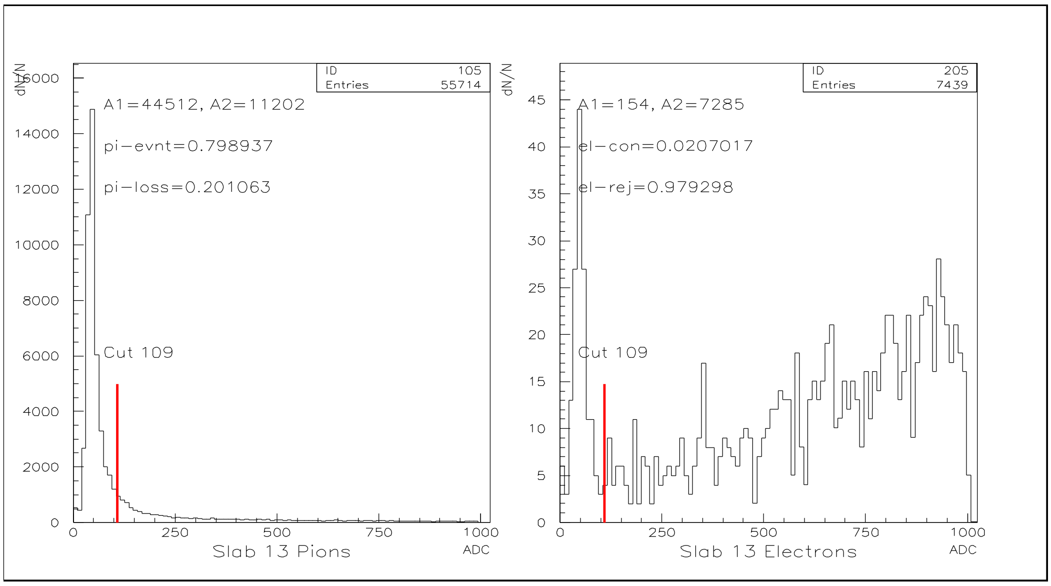

Figura 5 c. PSh Pion and Electron spectra, slab 13, right arm

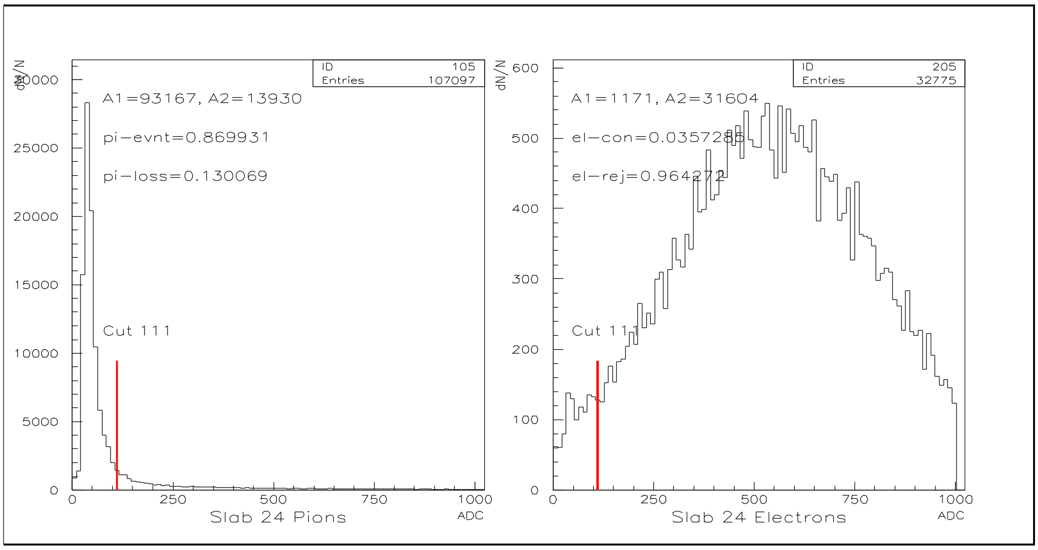

Figure 6 a. PSh Pion and Electron spectra, slab 4, left arm

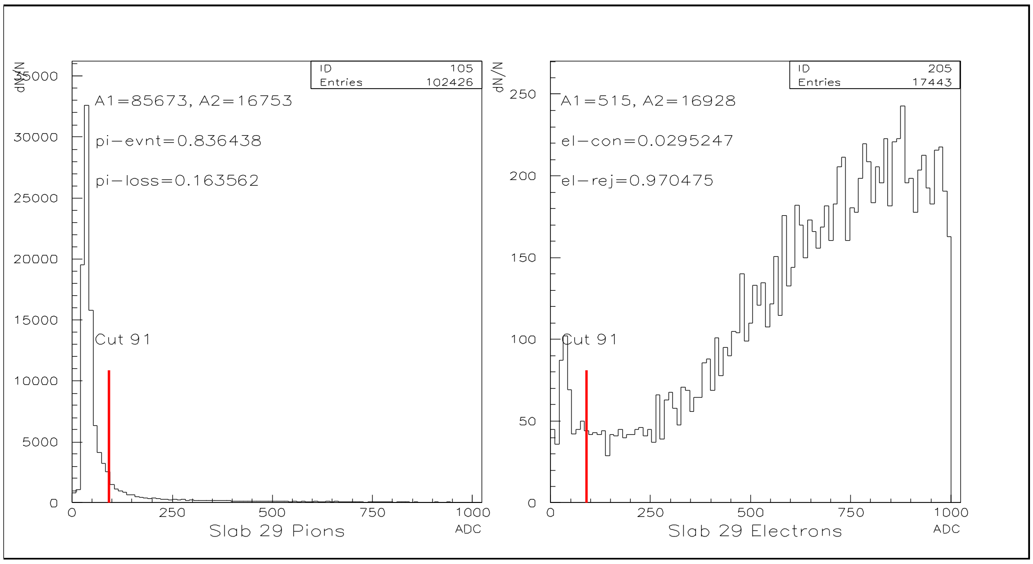

Figure 6 b. PSh Pion and Electron spectra, slab 9, left arm

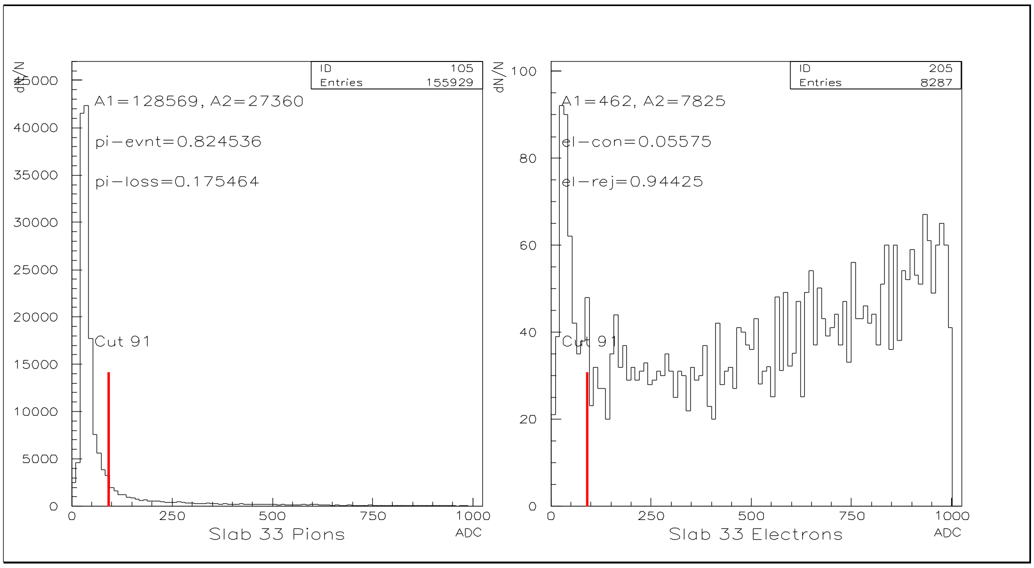

Figure 6 c. PSh Pion and Electron spectra, slab 13, left arm

Figures 5, 6 show pion and electron spectra with the measured A_1 and A_2 $(A_{tot}=A_1+A_2)$ values, and the ratios $\pi_{eff} = A_1^{\pi} / A_{tot}^{\pi}$ (pion detection efficiency) and $\pi_{loss} = A_2^{\pi} / A_{tot}^{\pi}$ (pion loss) as well as $\varepsilon_{esc} = A_1^{el} / A_{tot}^{el}$ (electron escape) and $\varepsilon_{rej} = A_2^{el} / A_{tot}^{el}$ (electron rejection).

Table 1 shows the π_{eff} values for all the 40 PSh slabs of the right arm (negative particles).

Table 2 shows the same π_{eff} values for the left arm (positive particule).

Table 3 shows the ε_{rej} values for all the 40 PSh slabs for the right arm (negative particles).

Table 4 shows the same ε_{rej} values for the left arm (positive particule).

Slabs 16-20 and 36-40 belong to the second layer, giving the amplitude signals from the shower produced after passing the first layer, slabs 11-15 and 31-35 (see **Figure 2, 3**).

Note ! The decrease in the rejection efficiency ε_{rej} and pion detection efficiency π_{eff} for both arms in the outermost slabs (1, 15 and 20), is due to the partial hit covering of the the detector surface (see **Figure 3** and **Figure 7**). Except of these values, the electron rejection efficiency ε_{rej} is greater than 90%.

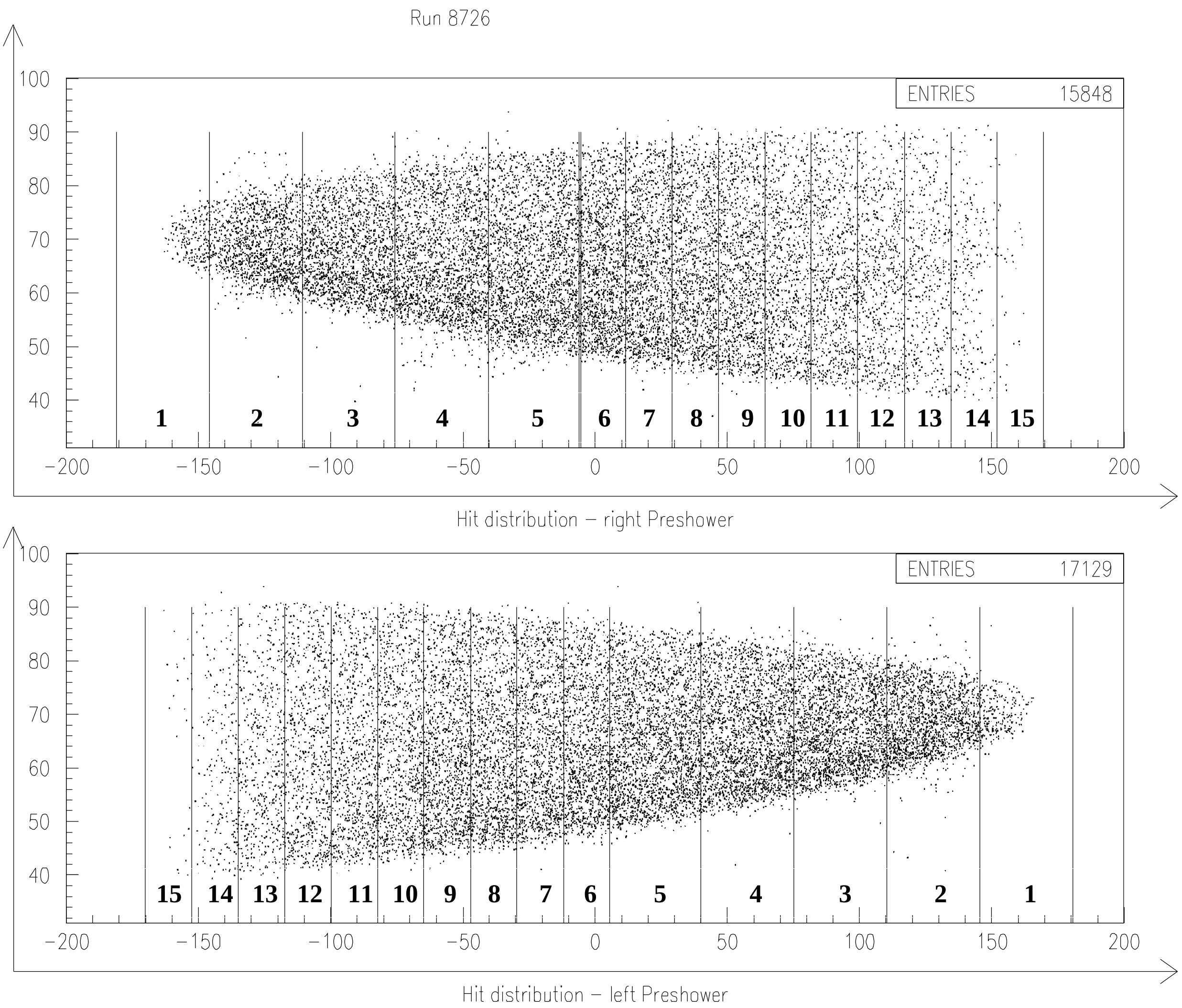

Figure 7. Hit distribution on the preshower.

Table 1

One layer preshower pion detection efficiency (right arm)

Slab Nr.	Cut	A_1^π	A_2^π	π_{eff1}	$\pm\sigma_{eff1}$	π_{esc1}	$\pm\sigma_{esc1}$
1	95	7344	765	0,9057	0,0146	0,0943	0,0036
2	87	68549	8629	0,8882	0,0047	0,1118	0,0013
3	98	107514	16746	0,8652	0,0036	0,1348	0,0011
4	105	146327	22493	0,8668	0,0031	0,1332	0,0009
5	108	183108	32103	0,8508	0,0027	0,1492	0,0009
6	93	103061	16424	0,8625	0,0037	0,1375	0,0011
7	94	108268	20506	0,8408	0,0035	0,1592	0,0012
8	92	117503	23074	0,8359	0,0033	0,1641	0,0012
9	106	124915	24723	0,8348	0,0032	0,1652	0,0011
10	102	133681	28129	0,8262	0,0031	0,1738	0,0011
11	81	92781	24329	0,7923	0,0035	0,2077	0,0015
12	104	68410	15567	0,8146	0,0042	0,1854	0,0016

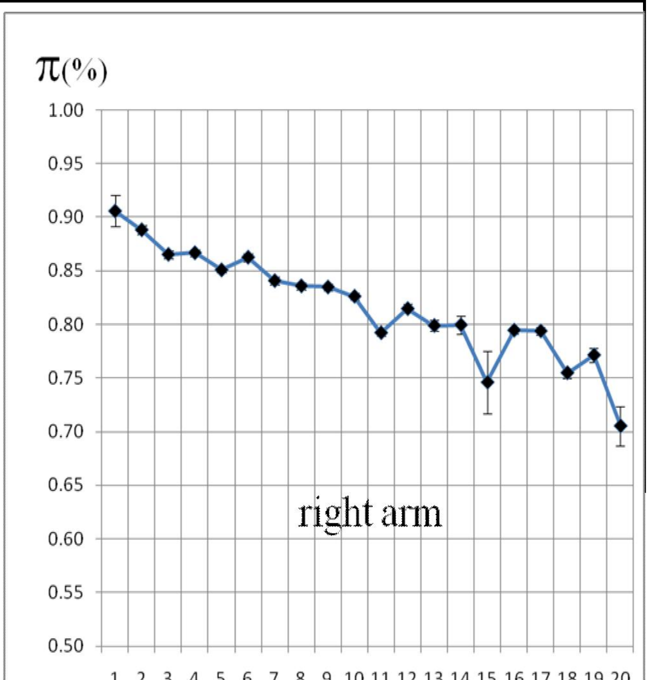

13	109	44512	11202	0,7989	0,0051	0,2011	0,0021
14	115	17256	4326	0,7996	0,0082	0,2004	0,0033
15	103	1178	401	0,7460	0,0287	0,2540	0,0142
16	94	95208	24616	0,7946	0,0034	0,2054	0,0014
17	98	66529	17278	0,7938	0,0041	0,2062	0,0017
18	98	44075	14314	0,7549	0,0048	0,2451	0,0023
19	99	21938	6501	0,7714	0,0069	0,2286	0,0031
20	76	2599	1086	0,7053	0,0181	0,2947	0,0102

Table 2

One layer preshower pion detection efficiency (left arm)

Slab Nr.	Cut	A_1^{π}	A_2^{π}	π_{eff1}	$\pm\sigma_{eff1}$	π_{esc1}	$\pm\sigma_{esc1}$
1	134	3562	325	0,9164	0,0213	0,0836	0,0048
2	137	39816	3084	0,9281	0,0065	0,0719	0,0013
3	110	67210	8238	0,8908	0,0047	0,1092	0,0013
4	111	93167	13930	0,8699	0,0039	0,1301	0,0012
5	99	121627	18705	0,8667	0,0034	0,1333	0,0010
6	81	65937	12136	0,8446	0,0045	0,1554	0,0015
7	81	73311	13038	0,8490	0,0043	0,1510	0,0014
8	83	80035	14766	0,8442	0,0041	0,1558	0,0014
9	91	85673	16753	0,8364	0,0039	0,1636	0,0014
10	81	97605	21790	0,8175	0,0035	0,1825	0,0013
11	99	115574	26888	0,8113	0,0032	0,1887	0,0013
12	91	136230	28021	0,8294	0,0030	0,1706	0,0011
13	91	128569	27360	0,8245	0,0031	0,1755	0,0012
14	98	95256	22620	0,8081	0,0035	0,1919	0,0014
15	98	20622	6151	0,7703	0,0071	0,2297	0,0032
16	62	98977	29439	0,7708	0,0033	0,2292	0,0015
17	94	126384	32601	0,7949	0,0030	0,2051	0,0012
18	123	124838	26843	0,8230	0,0031	0,1770	0,0012
19	100	104152	30300	0,7746	0,0032	0,2254	0,0014
20	113	37503	12134	0,7555	0,0052	0,2445	0,0025

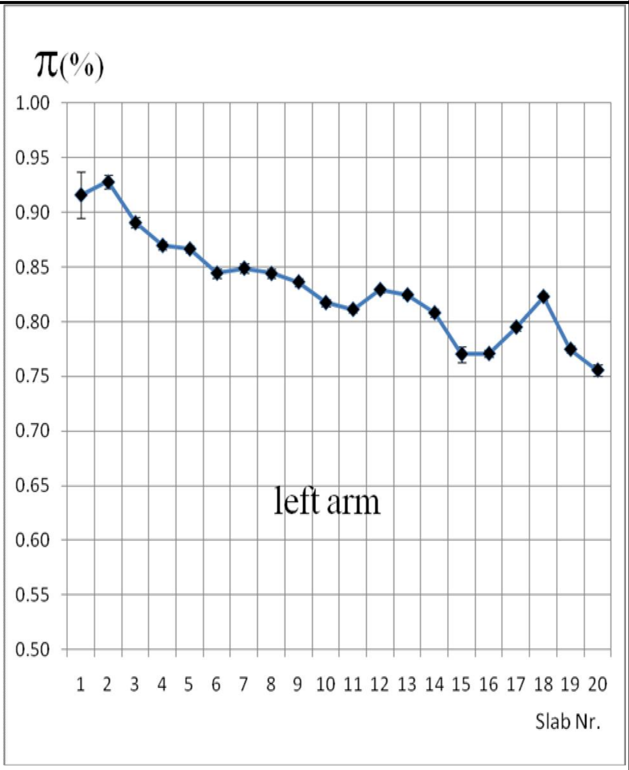

Table 3

One layer preshower electron rejection efficiency (right arm)

Slab Nr.	Cut	A_1^{el}	A_2^{el}	ε_{rej1}	$\pm\sigma_{rej1}$	ε_{esc1}	$\pm\sigma_{esc1}$
1	95	410	2984	0,8792	0,0221	0,1208	0,0063
2	87	1391	22091	0,9408	0,0088	0,0592	0,0016
3	98	1822	28634	0,9402	0,0077	0,0598	0,0014
4	105	1119	32070	0,9663	0,0076	0,0337	0,0010
5	108	818	34402	0,9768	0,0074	0,0232	0,0008
6	93	670	17378	0,9629	0,0102	0,0371	0,0015
7	94	529	17589	0,9708	0,0103	0,0292	0,0013
8	92	423	17557	0,9765	0,0104	0,0235	0,0012
9	106	355	17205	0,9798	0,0105	0,0202	0,0011
10	102	969	15034	0,9394	0,0107	0,0606	0,0020
11	81	502	13308	0,9636	0,0117	0,0364	0,0017
12	104	166	11077	0,9852	0,0132	0,0148	0,0012

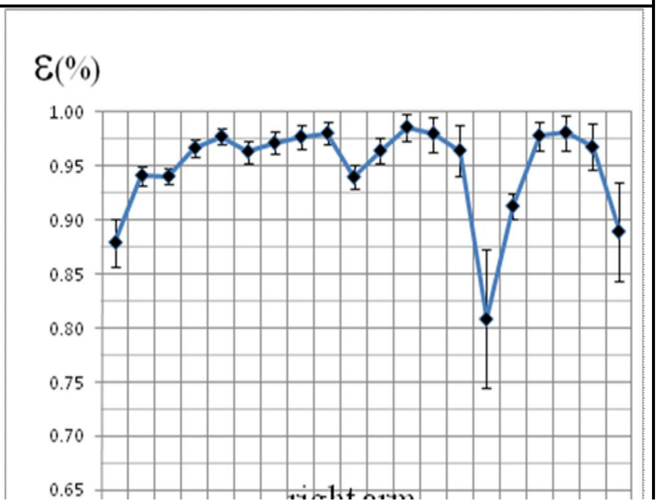

13	109	154	7285	0,9793	0,0161	0,0207	0,0017
14	115	125	3331	0,9638	0,0234	0,0362	0,0033
15	103	67	283	0,8086	0,0646	0,1914	0,0255
16	94	1191	12448	0,9127	0,0113	0,0873	0,0026
17	98	257	11183	0,9775	0,0130	0,0225	0,0014
18	98	157	7797	0,9803	0,0156	0,0197	0,0016
19	99	137	4017	0,9670	0,0214	0,0330	0,0029
20	76	90	723	0,8893	0,0455	0,1107	0,0123

Table 4

One layer preshower electron rejection efficiency (left arm)

Slab Nr.	Cut	A_1^{el}	A_2^{el}	ε_{rej1}	$\pm\sigma_{rej1}$	ε_{esc1}	$\pm\sigma_{esc1}$
1	134	523	2770	0,8412	0,0217	0,1588	0,0075
2	137	2465	20344	0,8919	0,0086	0,1081	0,0023
3	110	2355	27538	0,9212	0,0077	0,0788	0,0017
4	111	1171	31604	0,9643	0,0076	0,0357	0,0011
5	99	1038	33425	0,9699	0,0074	0,0301	0,0009
6	81	524	17377	0,9707	0,0103	0,0293	0,0013
7	81	526	17722	0,9712	0,0102	0,0288	0,0013
8	83	480	17443	0,9732	0,0104	0,0268	0,0012
9	91	515	16928	0,9705	0,0105	0,0295	0,0013
10	81	1295	14140	0,9161	0,0107	0,0839	0,0024
11	99	913	13332	0,9359	0,0113	0,0641	0,0022
12	91	508	11509	0,9577	0,0125	0,0423	0,0019
13	91	462	7825	0,9443	0,0149	0,0557	0,0027
14	98	296	3345	0,9187	0,0220	0,0813	0,0049
15	98	93	292	0,7584	0,0589	0,2416	0,0279
16	62	1238	12430	0,9094	0,0113	0,0906	0,0027
17	94	459	11579	0,9619	0,0125	0,0381	0,0018
18	123	576	8304	0,9351	0,0143	0,0649	0,0028
19	100	250	4213	0,9440	0,0203	0,0560	0,0036
20	113	148	640	0,8122	0,0432	0,1878	0,0168

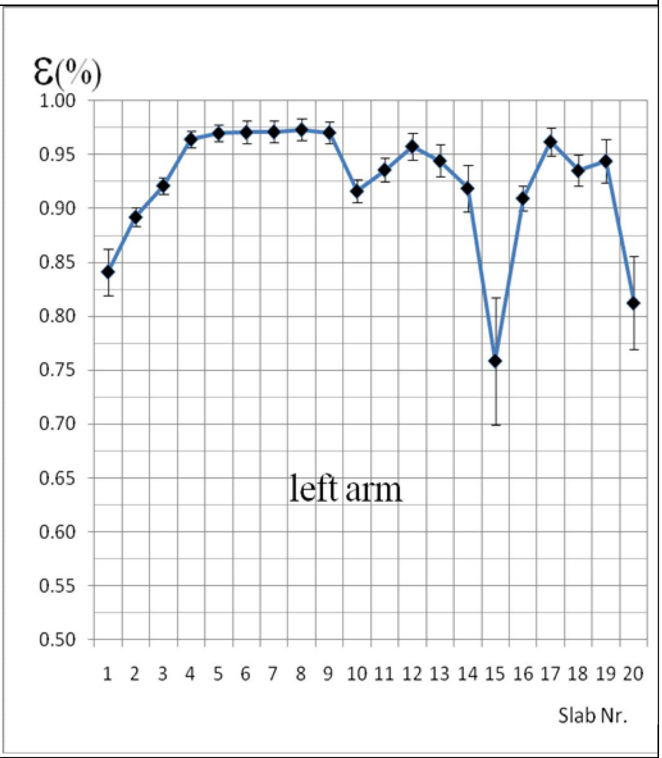

3. Two layers preshower detector efficiency.

To increase the preshower detector efficiency, a new layer has been added in the region of kaon phase space detection where the Cherenkov efficiency is lower (see **Figure 2, 3**). This second layer will detect the pions and electrons that cannot be detected or escape the first layer. The second preshower layer will process the high amplitude pions (higher then the cut level) and the low amplitude electrons (lower then the cut level).

Figure 8a shows the pion and electron spectra for the slab pairs 11+16 on the right arm.

Figure 8b shows the pion and electron spectra for the slab pairs 12+17 on the left arm.

For event (particle) selection with the signal in both the first and the second layer, we used additional equal momenta condition of the Drift Chamber tracks, for all detected pair events ($p_{11}=p_{16}$, $p_{12}=p_{17}$, $p_{13}=p_{18}$. etc.).

The pion spectra in the **Figures 8a** and **8b** in the first line - first position, are produced by the I-st layer, and the spectra in the first line - second position, are produced by the lost pions in the I-st layer and detected by the II-nd layer. The overall *pion detection efficiency* is:

$$\pi_{eff} = \pi_{eff\text{-}I} + \pi_{loss\text{-}I} * \pi_{eff\text{-}II}$$

The two layers *pion detection efficiency* π_{eff} values for the slab pairs 1=(11+16), 2=(12+17), 3=(13+18) and 4=(14+19) have been evaluated and ploted in the **Table 5** (right arm) and **Table 6** (left arm), along with the $\pi_{eff\text{-}I}$, $\pi_{eff\text{-}II}$ and $\pi_{loss\text{-}I}$ for each pair. The outermost pairs (15+20) for both arms are lower efficiency due to the partial hit covering of the corresponding detector surface. They have not been included in the analysis.

Similarly, the electron spectra of the **Figures 8a** and **Figures 8b** in the second line – first position, are produced by the I-st layer, and the spectra in the second line - second position, are produced by the escaped electrons in the I-st layer and detected by the II-nd layer. The overall *electron rejection efficiency* is:

$$\varepsilon_{rej} = \varepsilon_{rej\text{-}I} + \varepsilon_{esc\text{-}I} * \varepsilon_{rej\text{-}II}$$

The two layers *electron rejection efficiency* ε_{rej} values for the slab pairs 1=(11+16), 2=(12+17), 3=(13+18) and 4=(14+19) have been evaluated and ploted in the **Table 7** (right arm) and **Table 8** (left arm), along with the $\varepsilon_{rej\text{-}I}$ **,** $\varepsilon_{rej\text{-}II}$ and $\varepsilon_{esc\text{-}I}$ for each pair. The outermost pairs (15+20) for both arms are lower efficiency due to the partial hit covering of the corresponding detector surface. They have not been included in the analysis.

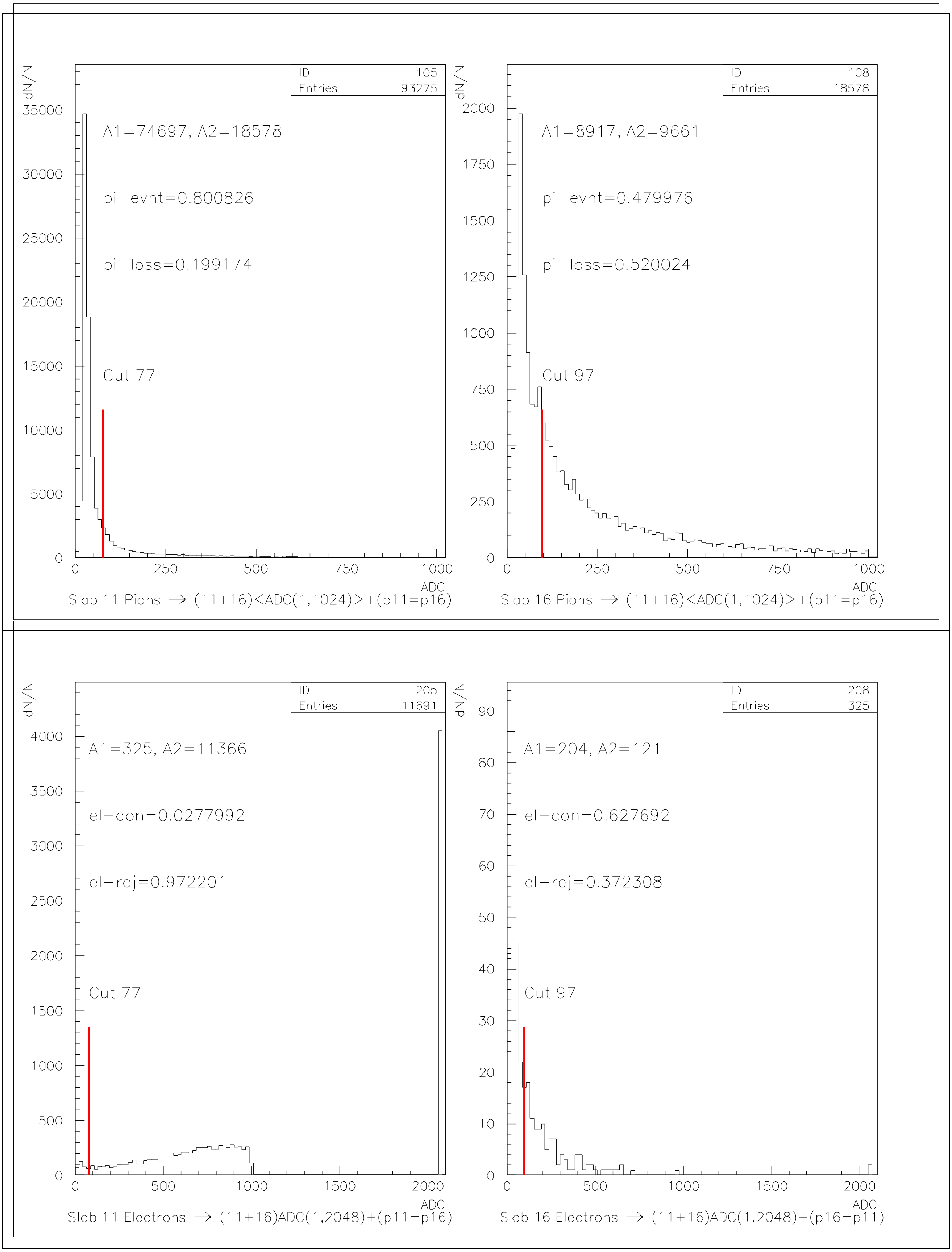

Figure 8 a. Two-layer PSh Pion and Electron spectra, slab 11 & 16, right arm

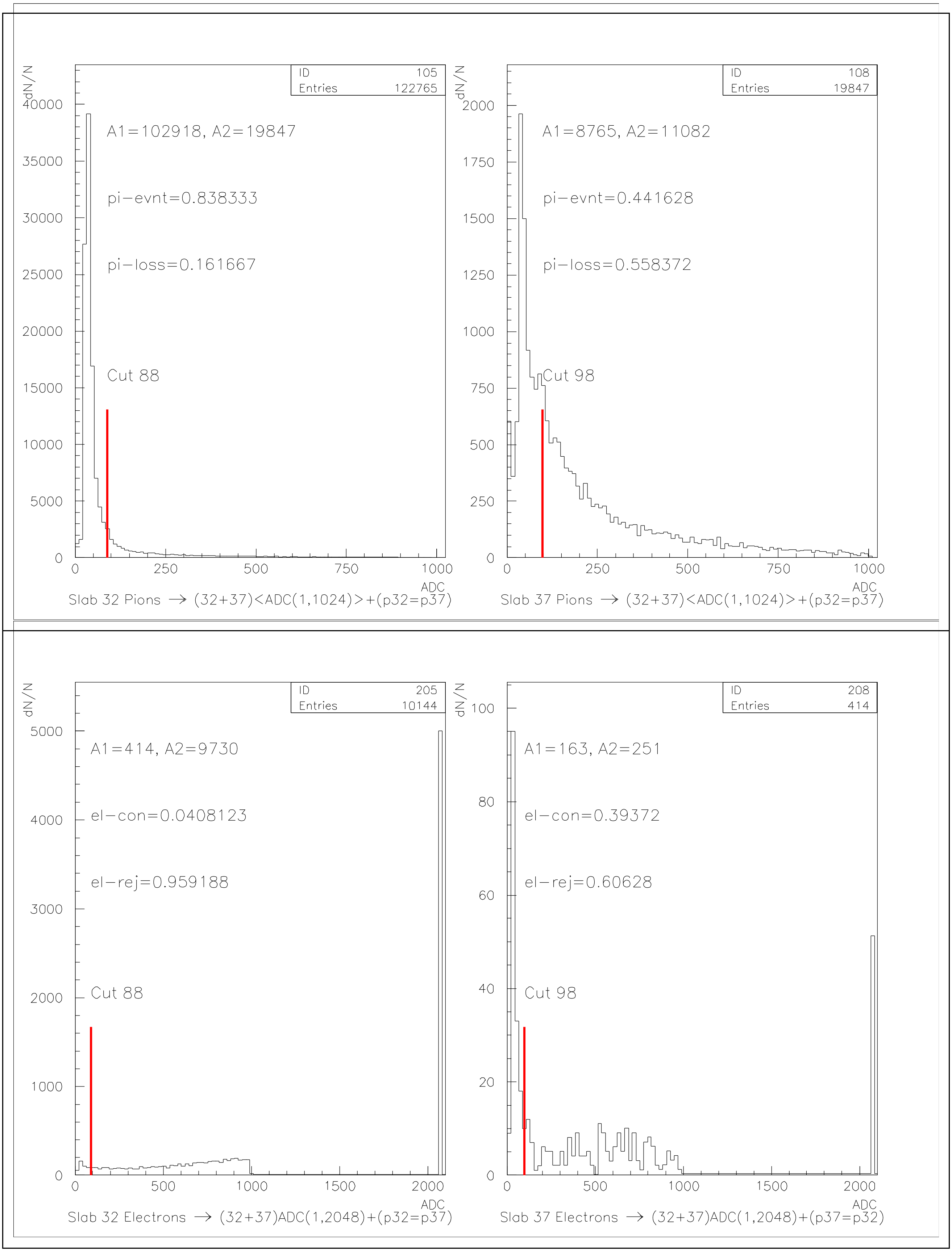

Figure 8 b. Two-layer PSh Pion and Electron spectra, slab 12 & 17, left arm

Table 5.

Two layers preshower pion detection efficiency (right arm)

Pair Nr.	1	2	3	4
Slab I/Slab II	11/ 16	12 / 17	13 / 18	14 / 19
Cut I/Cut II	77 / 97	101/104	107/103	112/103
$A_1^{\pi}(I)$	74697	54554	34744	14582
$A_2^{\pi}(I)$	18578	11421	8177	3428
$A_1^{\pi}(II)$	8917	5277	3469	1468
$A_2^{\pi}(II)$	9661	6144	4708	1960
$\pi_{eff\text{-}I}$	0,8008	0,8269	0,8095	0,8097
$\pm\sigma_{eff\text{-}I}$	0,0039	0,0048	0,0058	0,0090
$\pi_{eff\text{-}II}$	0,4800	0,4620	0,4242	0,4282
$\pm\sigma_{eff\text{-}II}$	0,0062	0,0077	0,0086	0,0134
$\pi_{loss\text{-}I}$	0,1992	0,1731	0,1905	0,1903
$\pm\sigma_{loss\text{-}I}$	0,0016	0,0018	0,0023	0,0035
$\pi_{loss\text{-}II}$	0,5200	0,5380	0,5758	0,5718
$\pm\sigma_{loss\text{-}II}$	0,0065	0,0085	0,0105	0,0162
$\pi_{eff\text{-}I}+\pi_{loss\text{-}I}*\pi_{eff\text{-}II}$	0,8964	0,9069	0,8903	0,8912
$\pm\sigma$	0,0042	0,0050	0,0061	0,0095

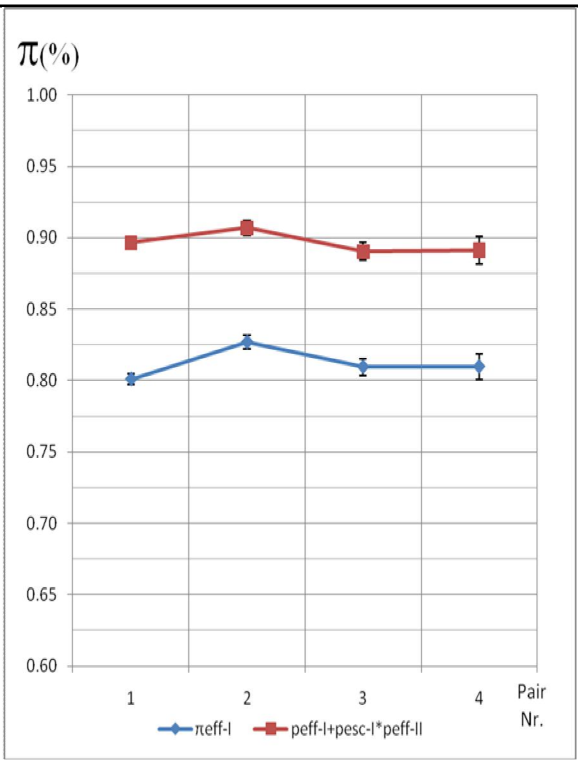

Table 6.

Two layers preshower pion detection efficiency (left arm)

Pair Nr.	1	2	3	4
Slab I/Slab II	11 / 16.	12 / 17.	13 / 18.	14 / 19.
Cut I/Cut II	96 / 65	88 / 98	88 / 129	96 / 104
$A_1^{\pi}(I)$	85304	102918	92893	72496
$A_2^{\pi}(I)$	18500	19847	18509	16289
$A_1^{\pi}(II)$	7998	8765	8796	6746
$A_2^{\pi}(II)$	10502	11082	9713	9543
$\pi_{eff\text{-}I}$	0,8218	0,8383	0,8339	0,8165
$\pm\sigma_{eff\text{-}I}$	0,0038	0,0035	0,0037	0,0041
$\pi_{eff\text{-}II}$	0,4323	0,4416	0,4752	0,4141
$\pm\sigma_{eff\text{-}II}$	0,0058	0,0057	0,0062	0,0060
$\pi_{loss\text{-}I}$	0,1782	0,1617	0,1661	0,1835
$\pm\sigma_{loss\text{-}I}$	0,0014	0,0012	0,0013	0,0016
$\pi_{loss\text{-}II}$	0,5677	0,5584	0,5248	0,5859
$\pm\sigma_{loss\text{-}II}$	0,0069	0,0066	0,0066	0,0076
$\pi_{eff\text{-}I}+\pi_{loss\text{-}I}*\pi_{eff\text{-}II}$	0,8988	0,9097	0,9128	0,8925
$\pm\sigma$	0,0040	0,0037	0,0039	0,0043

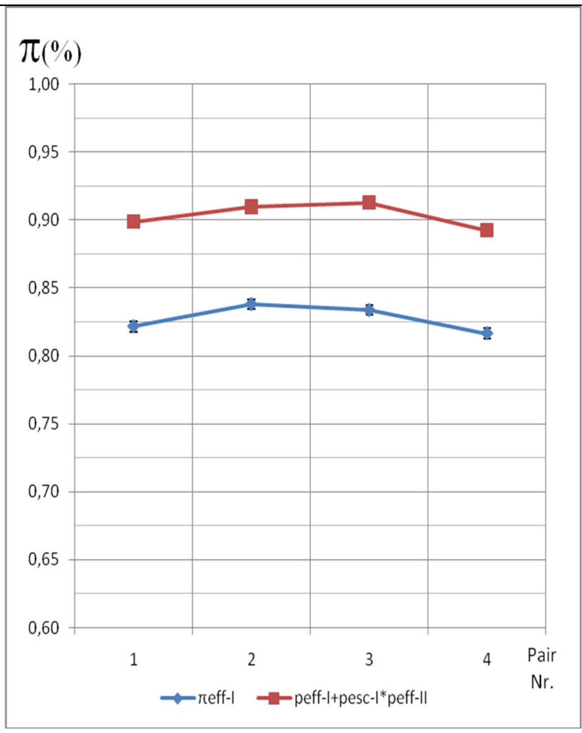

Table 7.

Two layers preshower electron rejection efficiency (rigtht arm)

Pair Nr.	1	2	3	4
Slab I/Slab II	11 / 16.	12 / 17.	13 / 18.	14 / 19.
Cut I/Cut II	77 / 97	101/104	107/103	112/103
$A_1^{el}(I)$	325	122	108	88
$A_2^{el}(I)$	11366	9393	6146	2898
$A_1^{el}(II)$	204	90	80	71
$A_2^{el}(II)$	121	32	28	17
ε_{rejI}	0,9722	0,9872	0,9827	0,9705
$\pm\sigma_{rejI}$	0,0128	0,0144	0,0177	0,0253
ε_{rejII}	0,3723	0,2623	0,2593	0,1932
$\pm\sigma_{rejII}$	0,0396	0,0521	0,0550	0,0512
ε_{escI}	0,0278	0,0128	0,0173	0,0295
$\pm\sigma_{escI}$	0,0016	0,0012	0,0017	0,0032
ε_{escII}	0,6277	0,7377	0,7407	0,8068
$\pm\sigma_{escII}$	0,0561	0,1025	0,1093	0,1287
$\varepsilon_{rejI}+\varepsilon_{escI}*\varepsilon_{rejII}$	0,9826	0,9905	0,9872	0,9762
$\pm\sigma$	0,0129	0,0144	0,0177	0,0254

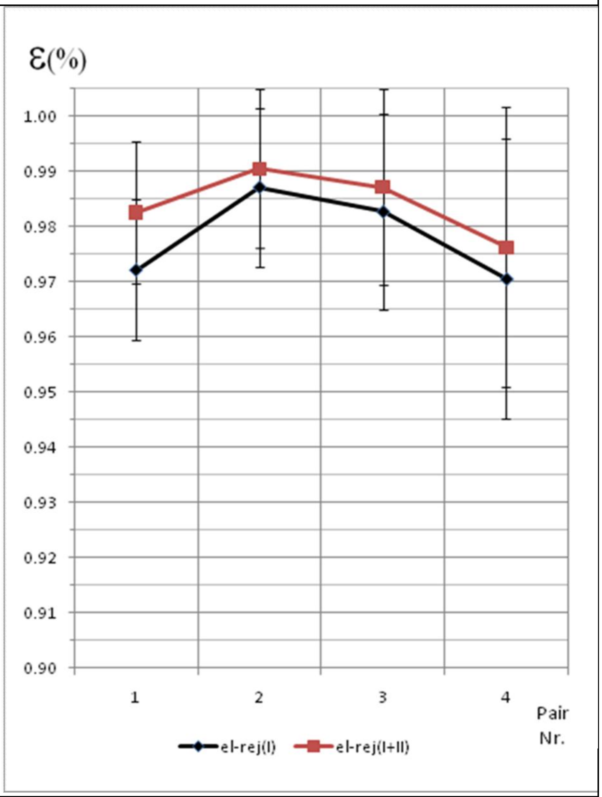

Table 8.

Two layers preshower electron rejection efficiency (left arm)

Pair Nr.	1	2	3	4
Slab I/Slab II	11 / 16.	12 / 17.	13 / 18.	14 / 19.
Cut I/Cut II	96 / 65	88 / 98	88 / 129	96 / 104
$A_1^{el}(I)$	653	414	380	222
$A_2^{el}(I)$	11360	9730	6629	2980
$A_1^{el}(II)$	312	163	209	129
$A_2^{el}(II)$	341	251	171	93
ε_{rejI}	0,9456	0,9592	0,9458	0,9307
$\pm\sigma_{rejI}$	0,0124	0,0136	0,0162	0,0237
ε_{rejII}	0,5222	0,6063	0,4500	0,4189
$\pm\sigma_{rejII}$	0,0349	0,0485	0,0414	0,0517
ε_{escI}	0,0544	0,0408	0,0542	0,0693
$\pm\sigma_{escI}$	0,0022	0,0020	0,0029	0,0048
ε_{escII}	0,4778	0,3937	0,5500	0,5811
$\pm\sigma_{escII}$	0,0329	0,0364	0,0474	0,0643
$\varepsilon_{rejI}+\varepsilon_{escI}*\varepsilon_{rejII}$	0,9740	0,9839	0,9702	0,9597
$\pm\sigma$	0,0126	0,0138	0,0164	0,0240

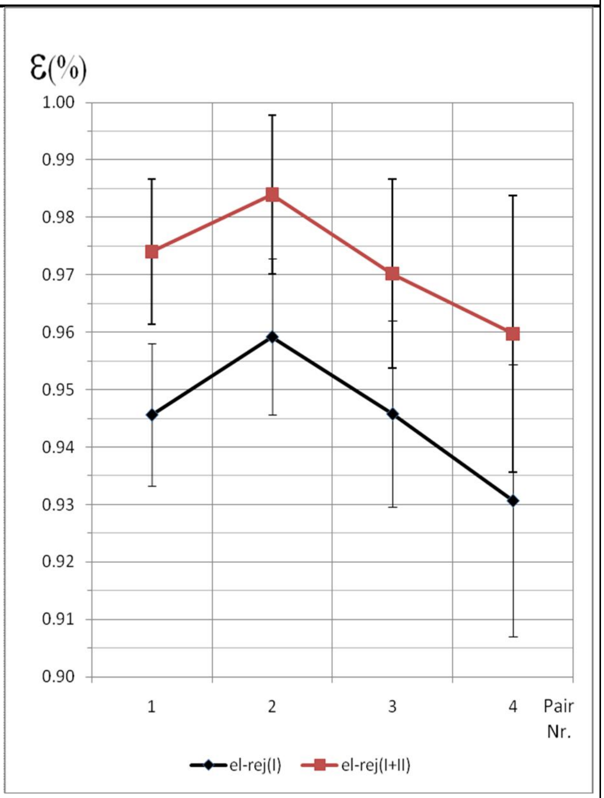

4. Electron rejection – pion efficiency correlation dependence on the cut channel position.

The cut channel position selection for each individual slab is essential for a good electron – pion separation. If the cut channel is lower than the optimal value, some pion events are lost and the pion efficiency π_{eff} is decreased, and if the cut position is higher, some electron events are escaped and the electron rejection efficiency ε_{rej} is decreased (see **Figures 5** and **6**).

Table 9 shows the particular values for π_{eff} for all the 40 PSh slabs and for different cut channels.

Table 10 shows the ε_{rej} values for the same 40 PSh slabs and the same cut channels as for pions**.**

Figures 9 present the $\pi_{eff} - \varepsilon_{rej}$ correlation for individual slabs and for some cut channel positions between 50 – 160.

Conclusion: The cut channel position determination for each individual slab is a difficult task if we are using such correlation diagrams, because they differ from slab to slab and also from run to run. The correlation diagrams are directly connected with the particular HV for each slab photomultiplier, and these values can change in time.

The optimal π_{eff} and ε_{rej} values, presented in the Section 2 and 3 have been evaluated automatically using a Gaussian fit of the pion peak. The cut channel position was fixed at about 7σ distance on the right side of this peak.

Table 9. (π-eff)

Slab Nr.	50	60	70	80	90	100	110	120	130	140	150	160
1	0.7313	0.8026	0.8468	0.8764	0.8958	0.9117	0.9222	0.9302	0.9353	0.9399	0.9450	0.9498
2	0.7547	0.8086	0.8492	0.8747	0.8937	0.9090	0.9191	0.9269	0.9324	0.9377	0.9416	0.9461
3	0.6562	0.7414	0.7946	0.8277	0.8494	0.8666	0.8792	0.8902	0.8989	0.9063	0.9131	0.9193
4	0.6462	0.7326	0.7850	0.8173	0.8396	0.8590	0.8738	0.8855	0.8941	0.9008	0.9074	0.9136
5	0.6106	0.7051	0.7624	0.7973	0.8201	0.8386	0.8534	0.8663	0.8769	0.8851	0.8927	0.8995
6	0.7178	0.7747	0.8121	0.8393	0.8564	0.8710	0.8813	0.8900	0.8971	0.9030	0.9084	0.9136
7	0.6517	0.7296	0.7791	0.8104	0.8331	0.8509	0.8637	0.8746	0.8831	0.8898	0.8966	0.9026
8	0.6682	0.7324	0.7782	0.8098	0.8322	0.8490	0.8617	0.8723	0.8802	0.8864	0.8926	0.8986
9	0.5559	0.6757	0.7438	0.7790	0.8022	0.8227	0.8395	0.8541	0.8650	0.8730	0.8801	0.8872
10	0.5975	0.6894	0.7446	0.7793	0.8020	0.8225	0.8383	0.8517	0.8609	0.8683	0.8759	0.8834
11	0.6836	0.7295	0.7658	0.7923	0.8095	0.8246	0.8364	0.8467	0.8544	0.8612	0.8683	0.8749
12	0.6022	0.6832	0.7312	0.7634	0.7865	0.8063	0.8213	0.8339	0.8435	0.8513	0.8586	0.8665
13	0.4960	0.6250	0.6948	0.7325	0.7581	0.7810	0.7989	0.8153	0.8278	0.8368	0.8453	0.8529
14	0.4211	0.5849	0.6670	0.7141	0.7414	0.7682	0.7900	0.8065	0.8208	0.8312	0.8413	0.8497
15	0.5826	0.6339	0.6770	0.7080	0.7296	0.7441	0.7574	0.7676	0.7783	0.7887	0.7980	0.8062
16	0.6099	0.6790	0.7264	0.7603	0.7852	0.8065	0.8227	0.8372	0.8481	0.8561	0.8647	0.8730
17	0.5963	0.6631	0.7137	0.7490	0.7742	0.7958	0.8106	0.8244	0.8355	0.8446	0.8538	0.8625
18	0.5284	0.6143	0.6677	0.7032	0.7314	0.7568	0.7771	0.7948	0.8076	0.8170	0.8271	0.8368
19	0.5830	0.6459	0.6944	0.7285	0.7529	0.7714	0.7848	0.7981	0.8097	0.8201	0.8302	0.8384
20	0.6062	0.6467	0.6893	0.7194	0.7408	0.7604	0.7777	0.7910	0.7997	0.8081	0.8149	0.8201
21	0.5632	0.6792	0.7746	0.8315	0.8590	0.8809	0.8914	0.9051	0.9120	0.9226	0.9303	0.9367
22	0.6501	0.7547	0.8228	0.8572	0.8779	0.8938	0.9063	0.9165	0.9246	0.9303	0.9354	0.9400
23	0.6959	0.7725	0.8206	0.8509	0.8667	0.8802	0.8908	0.8995	0.9072	0.9131	0.9183	0.9229
24	0.5922	0.7062	0.7698	0.8086	0.8340	0.8546	0.8688	0.8805	0.8897	0.8967	0.9027	0.9088
25	0.7070	0.7642	0.8078	0.8365	0.8535	0.8667	0.8763	0.8861	0.8935	0.8997	0.9056	0.9112
26	0.7259	0.7795	0.8184	0.8446	0.8621	0.8760	0.8854	0.8932	0.8996	0.9048	0.9096	0.9143
27	0.7382	0.7858	0.8247	0.8490	0.8631	0.8741	0.8823	0.8904	0.8964	0.9014	0.9070	0.9116
28	0.7171	0.7719	0.8103	0.8376	0.8556	0.8687	0.8785	0.8868	0.8935	0.8984	0.9034	0.9084
29	0.6626	0.7331	0.7790	0.8113	0.8326	0.8489	0.8605	0.8710	0.8789	0.8848	0.8908	0.8965
30	0.6971	0.7521	0.7904	0.8175	0.8364	0.8513	0.8626	0.8724	0.8799	0.8854	0.8908	0.8960
31	0.5619	0.6680	0.7310	0.7659	0.7901	0.8113	0.8270	0.8404	0.8509	0.8589	0.8663	0.8735
32	0.6756	0.7367	0.7810	0.8076	0.8261	0.8409	0.8519	0.8621	0.8694	0.8748	0.8806	0.8864
33	0.6834	0.7368	0.7781	0.8034	0.8215	0.8352	0.8463	0.8559	0.8632	0.8693	0.8750	0.8807
34	0.6041	0.6856	0.7347	0.7664	0.7894	0.8098	0.8244	0.8373	0.8471	0.8540	0.8610	0.8673
35	0.5942	0.6560	0.7000	0.7295	0.7528	0.7720	0.7886	0.8037	0.8146	0.8222	0.8321	0.8404
36	0.7179	0.7592	0.7983	0.8259	0.8423	0.8545	0.8643	0.8735	0.8815	0.8883	0.8955	0.9021
37	0.5812	0.6690	0.7232	0.7583	0.7855	0.8082	0.8252	0.8395	0.8500	0.8585	0.8670	0.8748
38	0.5073	0.6291	0.7028	0.7431	0.7689	0.7885	0.8039	0.8190	0.8314	0.8422	0.8519	0.8600
39	0.5168	0.6204	0.6827	0.7207	0.7500	0.7746	0.7937	0.8101	0.8214	0.8316	0.8410	0.8498
40	0.4547	0.5688	0.6419	0.6833	0.7091	0.7321	0.7504	0.7690	0.7823	0.7937	0.8045	0.8157

Table 10. (ε-rej)

Slab Nr.	50	60	70	80	90	100	110	120	130	140	150	160
1	0.9481	0.9355	0.9199	0.9039	0.8874	0.8698	0.8530	0.8353	0.8185	0.8008	0.7817	0.7631
2	0.9700	0.9626	0.9551	0.9469	0.9376	0.9254	0.9140	0.8996	0.8883	0.8777	0.8656	0.8515
3	0.9756	0.9694	0.9621	0.9550	0.9478	0.9397	0.9318	0.9225	0.9144	0.9062	0.8963	0.8844
4	0.9869	0.9840	0.9803	0.9763	0.9719	0.9679	0.9634	0.9584	0.9541	0.9495	0.9446	0.9390
5	0.9907	0.9886	0.9863	0.9840	0.9815	0.9791	0.9758	0.9730	0.9704	0.9682	0.9647	0.9611
6	0.9804	0.9761	0.9721	0.9683	0.9643	0.9616	0.9583	0.9549	0.9507	0.9470	0.9434	0.9390
7	0.9843	0.9815	0.9778	0.9752	0.9722	0.9694	0.9670	0.9651	0.9630	0.9606	0.9574	0.9537
8	0.9864	0.9841	0.9815	0.9796	0.9769	0.9742	0.9717	0.9691	0.9666	0.9642	0.9616	0.9592
9	0.9888	0.9868	0.9850	0.9837	0.9819	0.9805	0.9793	0.9775	0.9763	0.9745	0.9727	0.9712
10	0.9683	0.9619	0.9566	0.9515	0.9458	0.9406	0.9354	0.9296	0.9258	0.9214	0.9168	0.9121
11	0.9750	0.9702	0.9668	0.9636	0.9607	0.9570	0.9538	0.9505	0.9471	0.9433	0.9397	0.9351
12	0.9904	0.9887	0.9878	0.9869	0.9862	0.9853	0.9851	0.9843	0.9839	0.9832	0.9826	0.9812
13	0.9879	0.9847	0.9825	0.9812	0.9804	0.9798	0.9793	0.9784	0.9777	0.9771	0.9766	0.9754
14	0.9841	0.9766	0.9731	0.9708	0.9690	0.9670	0.9644	0.9635	0.9627	0.9621	0.9604	0.9604
15	0.8457	0.8371	0.8343	0.8229	0.8143	0.8114	0.8086	0.8029	0.7971	0.7943	0.7943	0.7943
16	0.9498	0.9409	0.9325	0.9247	0.9166	0.9086	0.9009	0.8919	0.8842	0.8766	0.8664	0.8559
17	0.9880	0.9857	0.9836	0.9816	0.9791	0.9771	0.9751	0.9727	0.9707	0.9694	0.9668	0.9635
18	0.9888	0.9873	0.9858	0.9835	0.9814	0.9800	0.9784	0.9767	0.9761	0.9736	0.9726	0.9712
19	0.9766	0.9747	0.9716	0.9701	0.9677	0.9670	0.9653	0.9644	0.9636	0.9624	0.9615	0.9593
20	0.9041	0.8979	0.8930	0.8868	0.8844	0.8795	0.8782	0.8721	0.8708	0.8696	0.8659	0.8610
21	0.9566	0.9402	0.9302	0.9180	0.9074	0.8916	0.8785	0.8621	0.8448	0.8333	0.8160	0.7971
22	0.9720	0.9653	0.9571	0.9484	0.9407	0.9314	0.9218	0.9106	0.8996	0.8883	0.8764	0.8624
23	0.9709	0.9642	0.9548	0.9454	0.9370	0.9282	0.9212	0.9108	0.9008	0.8905	0.8795	0.8666
24	0.9865	0.9831	0.9793	0.9761	0.9727	0.9688	0.9647	0.9605	0.9564	0.9523	0.9470	0.9413
25	0.9859	0.9834	0.9799	0.9765	0.9732	0.9699	0.9659	0.9612	0.9568	0.9532	0.9475	0.9411
26	0.9800	0.9775	0.9738	0.9707	0.9675	0.9641	0.9617	0.9585	0.9559	0.9518	0.9472	0.9421
27	0.9815	0.9779	0.9741	0.9712	0.9676	0.9650	0.9620	0.9585	0.9556	0.9529	0.9493	0.9455
28	0.9819	0.9794	0.9761	0.9737	0.9712	0.9679	0.9659	0.9635	0.9612	0.9587	0.9564	0.9534
29	0.9810	0.9787	0.9757	0.9730	0.9706	0.9686	0.9661	0.9633	0.9606	0.9592	0.9570	0.9545
30	0.9464	0.9361	0.9259	0.9161	0.9059	0.8974	0.8888	0.8785	0.8693	0.8622	0.8544	0.8475
31	0.9676	0.9611	0.9539	0.9473	0.9424	0.9359	0.9311	0.9259	0.9221	0.9184	0.9137	0.9094
32	0.9742	0.9695	0.9652	0.9615	0.9588	0.9541	0.9503	0.9460	0.9422	0.9390	0.9357	0.9323
33	0.9642	0.9587	0.9544	0.9499	0.9455	0.9415	0.9382	0.9342	0.9313	0.9283	0.9264	0.9201
34	0.9442	0.9390	0.9327	0.9280	0.9220	0.9184	0.9149	0.9105	0.9085	0.9052	0.9020	0.8962
35	0.8208	0.8026	0.7844	0.7818	0.7766	0.7584	0.7481	0.7377	0.7247	0.7195	0.7143	0.7091
36	0.9251	0.9128	0.8968	0.8794	0.8642	0.8498	0.8369	0.8238	0.8089	0.7931	0.7770	0.7586
37	0.9787	0.9747	0.9703	0.9668	0.9633	0.9588	0.9553	0.9515	0.9481	0.9450	0.9404	0.9355
38	0.9675	0.9617	0.9555	0.9507	0.9473	0.9431	0.9395	0.9365	0.9314	0.9269	0.9227	0.9178
39	0.9659	0.9603	0.9538	0.9498	0.9476	0.9440	0.9404	0.9375	0.9332	0.9287	0.9247	0.9196
40	0.8807	0.8566	0.8388	0.8299	0.8249	0.8185	0.8122	0.8109	0.8058	0.8033	0.7995	0.7970

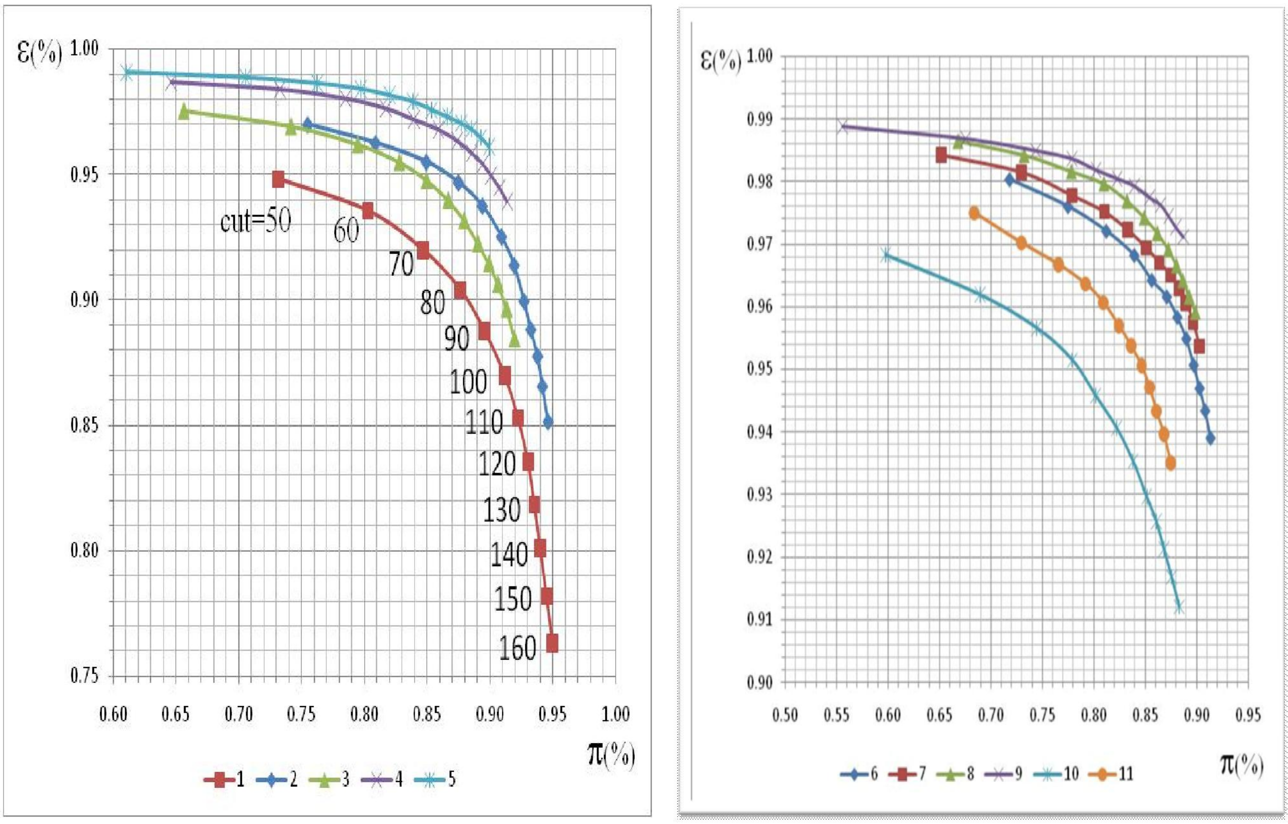

Figure 9a. Electron rejection (e) versus Pion detection efficiency (p) dependance on the Cut channel

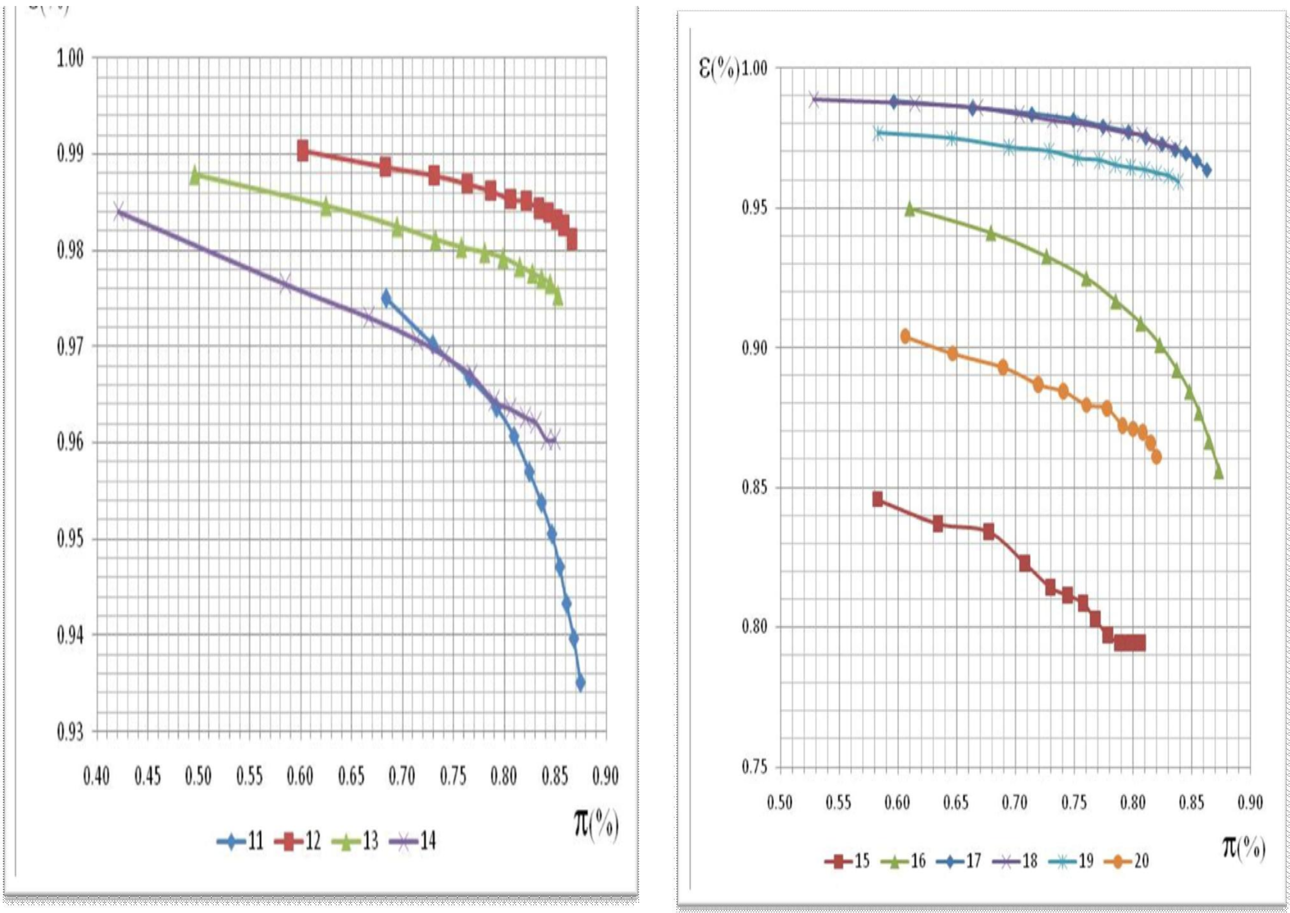

Figure 9b. Electron rejection (e) versus Pion detection efficiency (p) dependance on the Cut channel

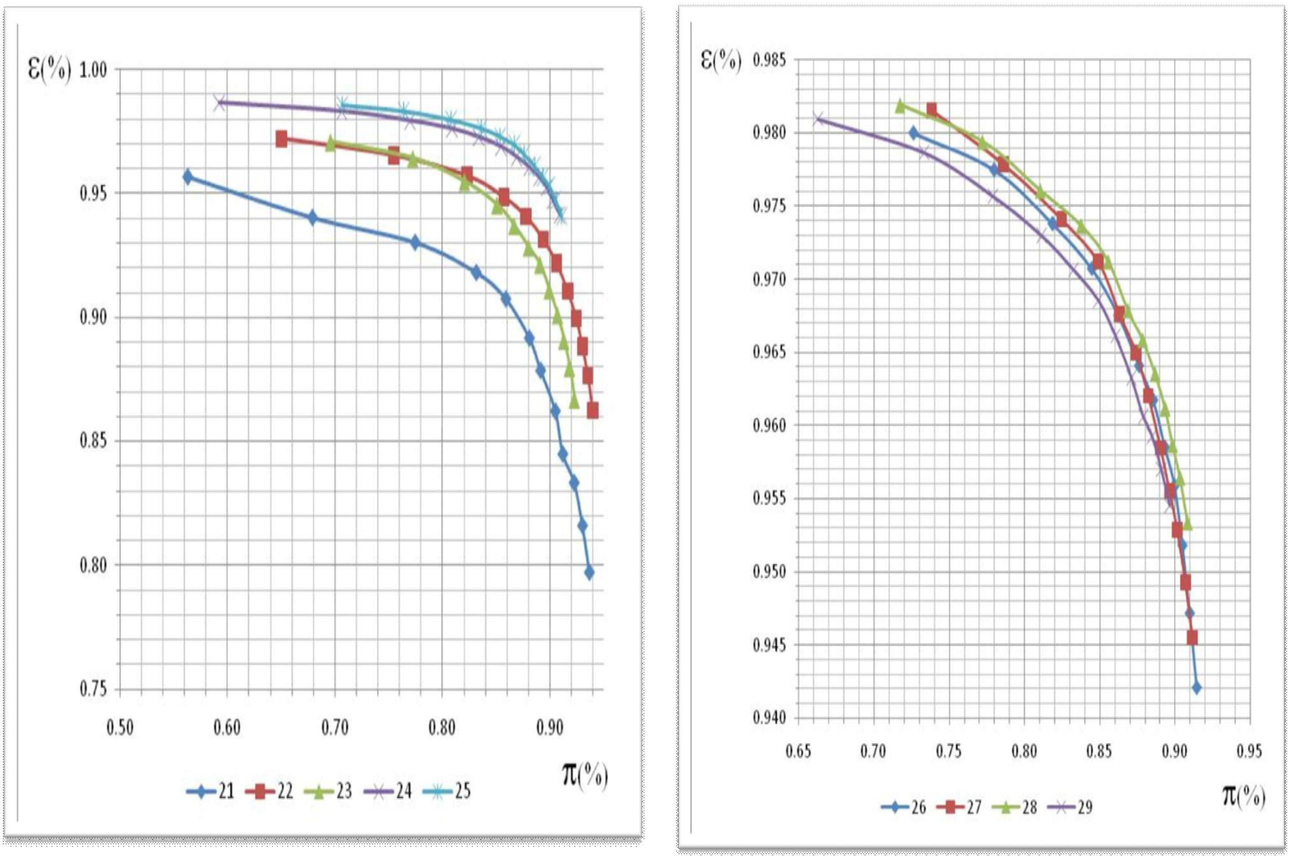

Figure 9c. Electron rejection (e) versus Pion detection efficiency (p) dependance on the Cut channel

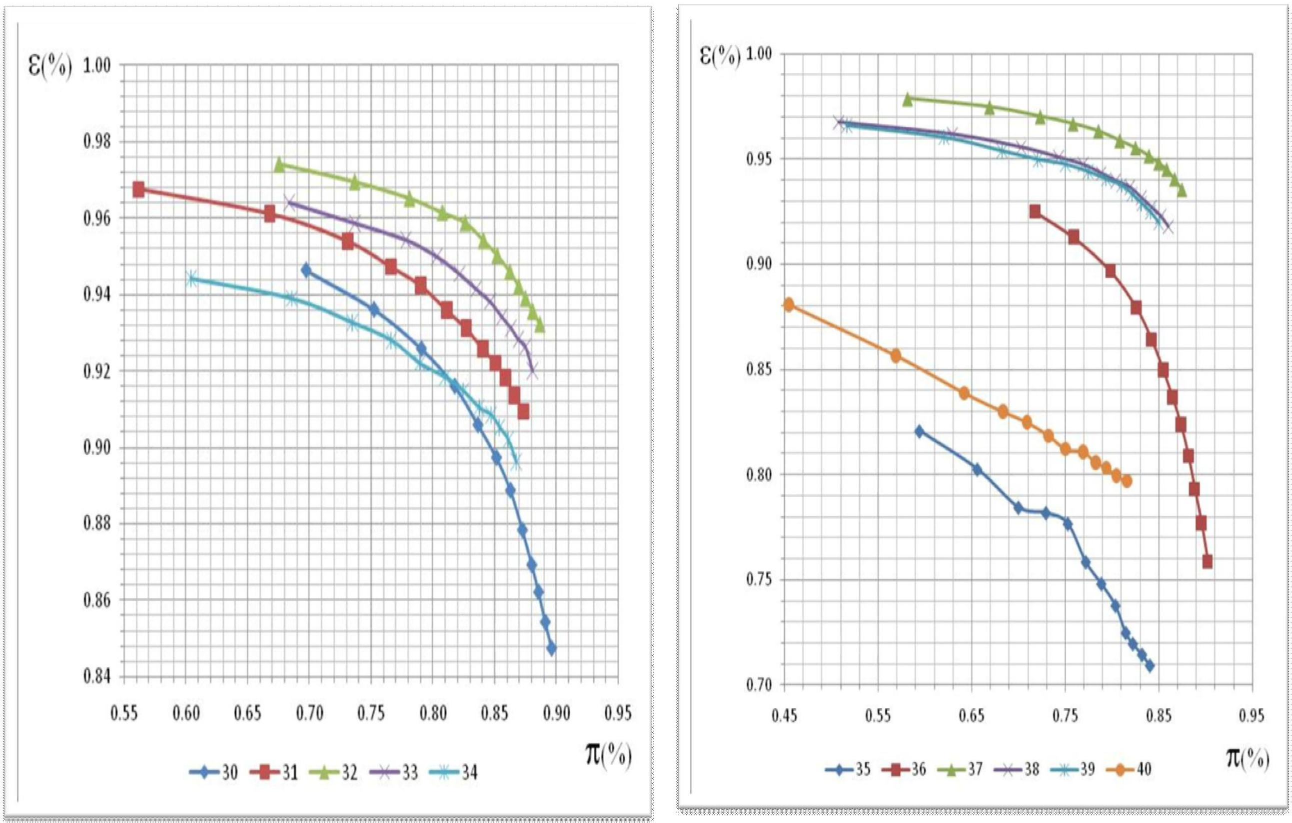

Figure 9d. Electron rejection (e) versus Pion detection efficiency (p) dependance on the Cut channel